EAI Endorsed Transactions
on Scalable Information Systems
EAI.EU Research Article

Direction-of-Arrival Estimation for Deterministic Networks

Feifei Hu*, Yu Huang, Xubin Lin, and Liu Wu

Power Dispatching and Control Center of China Southern Power Grid Co., Ltd., Guangzhou, China

Abstract

Direction-of-arrival (DOA) estimation is a key physical-layer technique for guaranteeing the stringent latency and reliability requirements of emerging deterministic networks. This paper investigates a generalized dual-subarray linear array model in which the inter-subarray displacement vectors can be arbitrarily specified, and devises two subspace-based DOA estimation schemes tailored to this setting. The first scheme is a spectral-search (SS) estimator that exploits the structured relationship between the signal subspaces of the two subarrays via a parametrized phase-rotation matrix, where the DOAs are obtained by searching over angles that induce a rank deficiency in a residual matrix constructed from the estimated signal subspace, yielding a high-resolution spectral function analogous to, but more flexible than the conventional schemes. The second scheme is a search-free (SF) estimator that, under mild geometric assumptions on the linear array, reformulates the same criterion as a polynomial in a complex exponential variable and recovers the DOAs from the roots closest to the unit circle, thereby eliminating grid search and significantly reducing computational complexity. Simulation results are provided for deterministic-network scenarios to show that, for a 2×5-element dual-subarray and moderate SNRs, the proposed SF-based estimator achieves an RMSE below 1 while conventional MUSIC exhibits an RMSE around 10, demonstrating roughly an order-of-magnitude accuracy gain and confirming the superior performance and scalability of the proposed SS and SF schemes.

Keywords: Deterministic networks, DOA estimation, performance evaluation.

Received on 05 June 2025; accepted on 26 November 2025; published on 8 December 2025

doi:10.4108/eetsis.9487

1. Introduction

Internet of Things (IoT) networks has gradually evolved from small, resource-constrained sensor networks to large-scale, heterogeneous infrastructures tightly integrated with the Internet and cloud/edge platforms [1–3]. In early studies, IoT networks were applied in low-power wireless sensor deployments, where energy-efficient routing, lightweight MAC protocols, and basic data aggregation were employed to extend network lifetime [4–6]. With the development of wireless communication, IoT architectures have been developed into perception, network, and application layers, and a range of wireless access technologies such as Wi-Fi, cellular systems, ZigBee, Bluetooth, and later LPWAN solutions like LoRaWAN and NB-IoT were proposed to satisfy diverse requirements on coverage, capacity, and power consumption. With the further introduction of cloud and edge/fog computing, IoT networks have been devised as distributed systems in which computation and storage are offloaded to remote servers or edge nodes, and issues such as latency reduction, scalable device management, and context-aware services have been investigated [7, 8]. More recently, IoT has been integrated with 5G/6G, SDN, and NFV, through which flexible network slicing, dynamic resource orchestration, and differentiated QoS for various applications have been enabled, while persistent challenges in security, privacy, and interoperability have continued to be highlighted and addressed by secure architectures, lightweight cryptography, and AI-driven network management schemes [9].

As a typical form of IoT networks, deterministic networks have been widely investigated as communication systems in which worst-case delay, jitter, and

*Corresponding author. Email: feifeihu2023@126.com

packet loss are tightly bounded so that time-critical flows are delivered with guaranteed quality of service rather than on a best-effort basis [10–12]. In recent year, deterministic behavior over Ethernet has been extensively studied in time-sensitive networking (TSN), where precise time synchronization, time-aware traffic shaping, and redundancy mechanisms were proposed on top of standard bridged Ethernet to support industrial control, in-vehicle communication, and professional audio/video streams [13–15]. At higher layers, deterministic networking is typically analyzed in terms of the IETF DetNet architecture, by which explicitly reserved paths, congestion-loss-free forwarding, and service protection were studied so that TSN-like guarantees were extended across routed IP/MPLS networks [16, 17]. Nowadays, deterministic networks are portrayed as an evolution from proprietary fieldbuses and time-triggered protocols toward converged, standards-based infrastructures, in which heterogeneous traffic classes are carried over shared links while isolation and predictability are ensured through scheduling, traffic classes, and increasingly SDN-based centralized configuration and management [18].

In the IoT networks and deterministic networks, multiple-antenna techniques have been increasingly recognized as key physical-layer enablers for meeting stringent reliability and latency requirements [19–21]. For low-power IoT devices and gateways, various multiple-input multiple-output (MIMO) and beamforming schemes have been analyzed under energy and hardware constraints, and spatial diversity and multiplexing gains have been shown to be exploitable so that reliability and throughput have been improved without large bandwidth expansion [22, 23]. In industrial IoT scenarios with TSN/DetNet-based deterministic transport, multi-antenna links have been designed and evaluated as a means by which fading-induced delay variation and packet errors have been reduced, thereby supporting tighter end-to-end latency and jitter bounds [24]. Furthermore, massive MIMO and coordinated multi-point transmission at 5G/6G base stations have been investigated as mechanisms through which dense IoT devices and time-critical flows have been spatially isolated and served with high reliability [25], and multi-antenna resources have been incorporated into cross-layer frameworks where scheduling, link adaptation, and network slicing for deterministic IoT services have been jointly optimized [26].

This paper considers a generalized dual-subarray linear array model with arbitrarily specified inter-subarray displacement vectors and develops two dedicated subspace-based DOA estimation schemes. The first is a spectral-search (SS) estimator that leverages the structured relationship between the signal subspaces of the two subarrays through a parametrized phase-rotation matrix; the DOAs are obtained by scanning over candidate angles that render a suitably constructed residual matrix rank-deficient, thereby producing a high-resolution spectrum that is analogous to, yet more flexible than, conventional approaches. The second is a search-free (SF) estimator which, under mild geometric constraints on the array, recasts the same criterion into a polynomial in a complex exponential variable and extracts the DOAs from the roots closest to the unit circle, thus avoiding grid search and markedly reducing computational complexity. Simulation results for deterministic-network scenarios demonstrate that, for a (2×5)-element dual-subarray at moderate SNRs, the proposed SF scheme attains an RMSE below 1, whereas conventional methods such as multiple signal classification (MUSIC) yield an RMSE on the order of 10, indicating roughly an order-of-magnitude improvement in accuracy and confirming the superior performance and scalability of both the SS and SF schemes.

2. Array Model

In this paper, we consider the system model of a linear array system in deterministic networks, where the sensors in the first and second subarrays are indexed by $1,\ldots,M$ and $M+1,\ldots,2M$, respectively. The relative displacement vectors between the m-th sensor in the first subarray and its corresponding sensor in the second subarray are known and precisely specified for all sensor indices $m = 1,\ldots,M$. These displacement vectors describe the geometric translation from one subarray to the other and play a crucial role in capturing the phase differences necessary for direction-of-arrival estimation. In addition, the displacement vectors (x_m, y_m) need not be identical across different sensors. That is, the displacement vector associated with each sensor pair can vary arbitrarily with m, thereby enabling a broader class of array geometries. In the conventional DOA setup, the displacement vector is uniform across all sensor pairs, i.e., for all m, the corresponding sensors in the two subarrays are separated by the same vector displacement. By relaxing this constraint, the generalized system allows the array to accommodate arbitrary displacements while still maintaining the mathematical analysis necessary for coherent subspace-based parameter estimation.

Assume that a total of L narrowband signals originating from far-field, uncorrelated sources impinge upon a dual-subarray sensor array. The array consists of two subarrays, each composed of M elements, leading to a combined array of size $2M$. The received signal vector at time instant t, denoted by $\mathbf{x}(t) \in \mathbb{C}^{2M\times 1}$, can be given by,

$$\mathbf{x}(t) = \mathbf{A}\mathbf{s}(t) + \mathbf{n}(t), \tag{1}$$

where $\mathbf{s}(t) \in \mathbb{C}^{L\times 1}$ represents the vector of complex-valued source signals, and $\mathbf{A} \in \mathbb{C}^{2M\times L}$ is the array manifold (or direction) matrix composed of steering vectors corresponding to the directions of arrival. Additionally, $\{\theta_1, \ldots, \theta_L\}$. $\mathbf{n}(t) \in \mathbb{C}^{2M\times 1}$ denotes the additive noise vector, subject to the temporally white and spatially uncorrelated with zero-mean and equal variance at each sensor.

To reflect the dual-subarray structure, the array manifold matrix $\mathbf{A}$ is partitioned into two submatrices,

$$\mathbf{A} = \begin{bmatrix} \mathbf{A}_1 \\ \mathbf{A}_2 \end{bmatrix}, \tag{2}$$

with

$$\mathbf{A}_1 = [\mathbf{a}(\theta_1), \ldots, \mathbf{a}(\theta_L)] \in \mathbb{C}^{M\times L}, \tag{3}$$

$$\mathbf{A}_2 = [\mathbf{\Phi}_1\mathbf{a}(\theta_1), \ldots, \mathbf{\Phi}_L\mathbf{a}(\theta_L)] \in \mathbb{C}^{M\times L}, \tag{4}$$

which represents the array response matrix of the first subarray and the modified response matrix of the second subarray, where each column is phase-shifted based on the sensor displacement between subarrays. Additionally, θ_l is the DOA of the l-th source signal with respect to the array axis, typically measured from the x-axis. The vector $\mathbf{a}(\theta) \in \mathbb{C}^{M\times 1}$ denotes the steering vector corresponding to direction θ for the first subarray, and the diagonal phase shift matrix $\mathbf{\Phi}_l \in \mathbb{C}^{M\times M}$ is given by,

$$\mathbf{\Phi}_l = \text{diag}\left\{e^{j\phi_{1l}}, \ldots, e^{j\phi_{Ml}}\right\}, \tag{5}$$

where the phase shift ϕ_{ml} applied to the m-th element for the l-th signal is,

$$\phi_{ml} = \frac{2\pi}{\lambda}\left(x_m \sin(\theta_l) + y_m \cos(\theta_l)\right), \tag{6}$$

where λ is the wavelength of the impinging signals. This configuration effectively models a generalized dual-subarray system, commonly used in applications such as direction-of-arrival estimation, radar signal processing, and array calibration, where spatial diversity and phase relationships are exploited to improve estimation accuracy.

To analyze the spatial characteristics of the received signal, the second-order statistical properties of the received array data is analyzed. Specifically, let $\mathbf{R} \in \mathbb{C}^{2M\times 2M}$ denote the spatial covariance matrix of the array output, defined as the expected outer product of the array snapshot vector $\mathbf{x}(t)$, i.e.,

$$\mathbf{R} = \mathbb{E}\left\{\mathbf{x}(t)\mathbf{x}^H(t)\right\}. \tag{7}$$

This covariance matrix can be decomposed via eigen-decomposition into the sum of two orthogonal components representing the signal and noise subspaces, respectively,

$$\mathbf{R} = \mathbf{E}\mathbf{\Lambda}\mathbf{E}^H + \mathbf{G}\mathbf{\Gamma}\mathbf{G}^H, \tag{8}$$

where $\mathbf{\Lambda} \in \mathbb{C}^{L\times L}$ is a diagonal matrix containing the L largest eigenvalues of $\mathbf{R}$, corresponding to the signal subspace, and $\mathbf{\Gamma} \in \mathbb{C}^{(2M-L)\times(2M-L)}$ is a diagonal matrix containing the remaining eigenvalues, associated with the noise subspace. Additionally, $\mathbf{E} \in \mathbb{C}^{2M\times L}$ is the matrix whose columns are the orthonormal eigenvectors spanning the signal subspace, and $\mathbf{G} \in \mathbb{C}^{2M\times(2M-L)}$ is the matrix whose columns are the orthonormal eigenvectors spanning the noise subspace. The superscript $(\cdot)^H$ denotes the Hermitian operator of conjugate transpose, and $\mathbb{E}\{\cdot\}$ returns the statistical expectation. This eigendecomposition plays a fundamental role in subspace-based direction-of-arrival estimation techniques, as it enables the separation of the signal and noise in the measurement space.

3. Spectral Search (SS) Based DOA Estimation

To exploit the structure of the array and the spatial characteristics of the incoming signals, the signal subspace matrix $\mathbf{E} \in \mathbb{C}^{2M\times L}$ is decomposed into two partitions associated with the dual-subarray configuration, given by,

$$\mathbf{E} = \begin{bmatrix} \mathbf{E}_1 \\ \mathbf{E}_2 \end{bmatrix}, \tag{9}$$

where $\mathbf{E}_1 \in \mathbb{C}^{M\times L}$ and $\mathbf{E}_2 \in \mathbb{C}^{M\times L}$ denote the submatrices corresponding to the signal subspaces of the first and second subarrays, respectively. Building upon the conventional estimation theory, we assume that the signal subspace matrix $\mathbf{E}$ lies in the column space of the array manifold matrix $\mathbf{A} \in \mathbb{C}^{2M\times L}$. Thus, it can be expressed as,

$$\mathbf{E} = \mathbf{A}\mathbf{T}, \tag{10}$$

where $\mathbf{T} \in \mathbb{C}^{L\times L}$ is a full-rank, non-singular transformation matrix representing the basis change between the array manifold and the signal subspace. Substituting the partitioned form of $\mathbf{A}$, we can obtain,

$$\mathbf{E}_1 = \mathbf{A}_1\mathbf{T}, \tag{11}$$

$$\mathbf{E}_2 = \mathbf{A}_2\mathbf{T}. \tag{12}$$

To proceed with the spectral search-based approach, we introduce a parametric diagonal matrix $\mathbf{\Psi}(\theta) \in \mathbb{C}^{M\times M}$, which captures the phase rotation due to sensor displacement with respect to a given direction of arrival θ. This matrix is given by,

$$\mathbf{\Psi}(\theta) = \text{diag}\left\{e^{j\psi_1}, \ldots, e^{j\psi_M}\right\}, \tag{13}$$

with the phase shift ψ_m for the m-th sensor expressed as,

$$\psi_m = \frac{2\pi}{\lambda}\left(x_m \sin(\theta) + y_m \cos(\theta)\right). \tag{14}$$

By leveraging this equation, we can define a residual matrix,

$$\mathbf{E}_2 - \mathbf{\Psi}\mathbf{E}_1 = \mathbf{Q}\mathbf{T}, \tag{15}$$

where the matrix $\mathbf{Q} \in \mathbb{C}^{M\times L}$ encapsulates the difference between the actual second subarray response and the hypothetical response obtained via phase-rotated first subarray elements. Specifically, $\mathbf{Q}$ is given by,

$$\mathbf{Q} = \left[(\mathbf{\Phi}_1 - \mathbf{\Psi})\mathbf{a}(\theta_1), \ldots, (\mathbf{\Phi}_L - \mathbf{\Psi})\mathbf{a}(\theta_L)\right]. \tag{16}$$

This equation serves as the foundation for spectral search-based DOA estimation. By sweeping over candidate DOA angles θ, the goal is to find those directions that minimize the norm of the residual $\|\mathbf{E}_2 - \mathbf{\Psi}(\theta)\mathbf{E}_1\|$, thereby identifying the true angles of arrival. The l-th column of the matrix $\mathbf{Q}$, as defined in the right-hand side of (15), will become identically zero when the angular parameter θ is exactly equal to the source direction of arrival. Specifically, if the number of sources L is less than or equal to the number of array elements in one subarray M, i.e., $L \leq M$, then the matrix difference $\mathbf{E}_2 - \mathbf{\Psi}(\theta)\mathbf{E}_1$ will experience a drop in rank when $\theta = \theta_l$.

Given that both $\mathbf{E}_1$ and $\mathbf{E}_2$ are tall matrices (i.e., more rows than columns), this rank deficiency can be detected through a subspace projection approach. In particular, we can identify the DOAs by searching for values of θ that induce a rank deficiency in the projected matrix difference,

$$\mathbf{W}^H\mathbf{E}_2 - \mathbf{W}^H\mathbf{\Psi}(\theta)\mathbf{E}_1, \tag{17}$$

where $\mathbf{W} \in \mathbb{C}^{M\times L}$ is an arbitrary full-rank matrix. The choice of $\mathbf{W}$ can affect the numerical stability and performance of the algorithm. To maintain consistency with the standard DOA estimation, we adopt $\mathbf{W} = \mathbf{E}_1$ in this work. With this selection, we define the spectral search function $f(\theta)$, which serves as the objective for identifying the source DOAs by locating its peaks, or equivalently, the valleys in the denominator. The function is defined as,

$$f(\theta) = \frac{1}{\det\left\{\mathbf{E}_1^H\mathbf{E}_2 - \mathbf{E}_1^H\mathbf{\Psi}(\theta)\mathbf{E}_1\right\}}, \tag{18}$$

where $\det(\mathbf{A})$ returns the determinant of matrix $\mathbf{A}$. This spectral function evaluates the closeness of $\mathbf{\Psi}(\theta)$ to matching the empirical phase shift between subarrays and thereby allows for high-resolution estimation of the source directions. Note that the structure of (18) shares conceptual similarities with the RARE receiver, which also leverages the idea of rank deficiency for DOA estimation. However, unlike the proposed approach, RARE is more closely related to the MUSIC algorithm in that it relies on a projection onto the signal subspace rather than the direct subspace alignment. Therefore, although both methods use rank-based criteria, RARE represents a generalization of MUSIC, while our approach remains rooted in the signal space.

In practical scenarios, the array data is obtained over a finite number of temporal snapshots. Consequently, the true covariance matrix $\mathbf{R}$ should be estimated empirically from the available data. Let K denote the number of such snapshots. Then, the sample covariance matrix $\hat{\mathbf{R}} \in \mathbb{C}^{2M\times 2M}$ is computed as,

$$\hat{\mathbf{R}} = \frac{1}{K}\sum_{t=1}^{K}\mathbf{x}(t)\mathbf{x}^H(t). \tag{19}$$

This matrix represents the standard sample mean estimator, which approximates the true statistical expectation under the assumption of ergodicity and stationarity. To facilitate subspace-based DOA estimation, we apply an eigendecomposition to the sample covariance matrix $\hat{\mathbf{R}}$, analogous to the decomposition of $\mathbf{R}$ in the asymptotic case, which results in,

$$\hat{\mathbf{R}} = \hat{\mathbf{E}}\hat{\mathbf{\Lambda}}\hat{\mathbf{E}}^H + \hat{\mathbf{G}}\hat{\mathbf{\Gamma}}\hat{\mathbf{G}}^H, \tag{20}$$

where $\hat{\mathbf{\Lambda}} \in \mathbb{C}^{L\times L}$ is a diagonal matrix consisting of the estimated signal-subspace eigenvalues, and $\hat{\mathbf{\Gamma}} \in \mathbb{C}^{(2M-L)\times(2M-L)}$ contains the estimated noise-subspace eigenvalues. Additionally, $\hat{\mathbf{E}} \in \mathbb{C}^{2M\times L}$ and $\hat{\mathbf{G}} \in \mathbb{C}^{2M\times(2M-L)}$ are the corresponding orthonormal eigenvector matrices spanning the estimated signal and noise subspaces, respectively. From $\hat{\mathbf{E}}$, we extract its upper and lower subarrays corresponding to the two subarrays of the physical array,

$$\hat{\mathbf{E}} = \begin{bmatrix}\hat{\mathbf{E}}_1 \\ \hat{\mathbf{E}}_2\end{bmatrix}. \tag{21}$$

Utilizing this eigendecomposition, the finite-sample approximation of the spectral function used for DOA estimation becomes,

$$f(\theta) = \frac{1}{\det\left\{\hat{\mathbf{E}}_1^H\hat{\mathbf{E}}_2 - \hat{\mathbf{E}}_1^H\mathbf{\Psi}(\theta)\hat{\mathbf{E}}_1\right\}}. \tag{22}$$

This expression quantifies the deviation between the empirical phase evolution captured in $\hat{\mathbf{E}}_2$ and the hypothetical phase shift induced by a test direction θ applied to $\hat{\mathbf{E}}_1$. The function $f(\theta)$ will exhibit peaks at the true DOAs, which correspond to the angles θ_l where the denominator matrix becomes rank-deficient or near-singular, indicating alignment between measured and modeled spatial responses. This finite-sample

Algorithm 1 Spectral-Search (SS) DOA Estimation

Input: Snapshots $\{\mathbf{x}(t)\}$, subarray geometry, wavelength λ, source number L, angle grid Θ
Output: Estimated DOAs $\{\hat{\theta}_\ell\}$
Subspace Estimation: Compute sample covariance $\hat{\mathbf{R}}$, perform EVD, and obtain signal subspace $\hat{\mathbf{E}}$
for each $\theta \in \Theta$ **do**
    Construct phase-rotation matrix $\boldsymbol{\Psi}(\theta) = \text{diag}(e^{j\psi_m(\theta)})$
    Form residual matrix $\mathbf{D}(\theta) = \hat{\mathbf{E}}_1^H \hat{\mathbf{E}}_2 - \hat{\mathbf{E}}_1^H \boldsymbol{\Psi}(\theta) \hat{\mathbf{E}}_1$
    Compute spectral value $f(\theta) = 1/\det(\mathbf{D}(\theta))$
end for
Peak Search: Identify L largest peaks of $f(\theta)$ to obtain $\{\hat{\theta}_\ell\}$

spectral search approach is summarized in Algorithm 1, which provides a robust and computationally efficient alternative to full parameter estimation, while preserving the subspace orthogonality principles foundational to high-resolution array signal processing techniques.

4. Search-Free (SF) DOA Estimation

The spectral estimator in (22) requires an exhaustive search over the angular domain θ, which is computationally intensive, especially in high-resolution scenarios or when dealing with a large number of snapshots. To mitigate this computational burden, we now propose a more efficient alternative of a search-free variant of the generalized DOA estimator. This approach is based on polynomial rooting and leverages the underlying array geometry to reformulate the problem algebraically.

To construct such an estimator, we impose structural assumptions on the array geometry for analytical tractability. Specifically, we assume that the y-component y_m of the displacement vector for each sensor in the second subarray is zero, i.e., $y_m = 0$ for all $m = 1, \ldots, M$. This implies that the array lies entirely along the x-axis, forming a one-dimensional linear structure. Without loss of generality, we also assume that the x-coordinates of the sensors are ordered in ascending order of $x_1 \le x_2 \le \cdots \le x_M$. Such an ordering is always possible through appropriate indexing of the array elements. Under these assumptions, the phase shift ψ_m introduced by the m-th sensor can be expressed relative to that of the first sensor, given by,

$$\psi_m = \frac{x_m}{x_1}\psi_1. \tag{23}$$

By introducing the substitution $z = e^{j\psi_1}$, we can define a parameterized diagonal matrix $\boldsymbol{\Psi}(z)$, which captures the relative phase shifts induced across the array,

$$\boldsymbol{\Psi}(z) = \text{diag}\left\{z^{\frac{x_2}{x_1}}, z^{\frac{x_3}{x_1}}, \ldots, z^{\frac{x_M}{x_1}}\right\}. \tag{24}$$

Substituting $\boldsymbol{\Psi}(z)$ into the spectral function, the denominator becomes a polynomial in z. Thus, the determinant-based expression transforms into,

$$p(z) = \det\left\{\hat{\mathbf{E}}_1^H \hat{\mathbf{E}}_2 - \hat{\mathbf{E}}_1^H \boldsymbol{\Psi}(z) \hat{\mathbf{E}}_1\right\}. \tag{25}$$

The zeros of this polynomial correspond to the exponentiated phase shifts $z = e^{j\psi_1}$, from which the DOAs can be recovered directly without grid-based search. Notably, if all the ratios x_m/x_1 (for $m = 1, \ldots, M$) are integers, then $p(z)$ becomes a polynomial in the usual algebraic sense with integer exponents, allowing standard polynomial root-finding techniques to be applied. More generally, even if the ratios x_m/x_1 are not integers, but there exists a common scaling factor c such that $c \cdot (x_m/x_1) \in \mathbb{Z}$ for all m, the method can still be applied by redefining $z = e^{j\psi_1/c}$ and forming a polynomial of degree $c \cdot \max(x_m/x_1)$. Thus, this polynomial rooting approach provides a powerful and computationally efficient alternative for estimating the DOAs in array processing systems.

In practice, the data is available only over a finite number of snapshots, and thus the polynomial derived in (25) should be evaluated using sample-based subspace estimates. In the finite sample case, the polynomial expression becomes,

$$p(z) = \det\left\{\hat{\mathbf{E}}_1^H \hat{\mathbf{E}}_2 - \hat{\mathbf{E}}_1^H \boldsymbol{\Psi}(z) \hat{\mathbf{E}}_1\right\}. \tag{26}$$

The roots of the polynomial $p(z)$ above provide critical information for DOA estimation. Specifically, the DOAs can be inferred from the L roots of $p(z)$ that lie closest to the unit circle in the complex plane. This is analogous to the root-MUSIC algorithm, where signal DOAs are estimated from the angles of unit-norm roots of a related polynomial derived from the MUSIC spectrum.

To establish a connection with the conventional DOA estimation, a special case in which all sensors in the second subarray are displaced identically in space is considered, i.e.,

$$x_1 = x_2 = \cdots = x_M. \tag{27}$$

Under this uniform displacement configuration, the phase shifts across all sensors become equal, and the parameterized diagonal matrix simplifies to a scalar multiplication by z. Consequently, the polynomial in (26) reduces to,

$$p(z) = \det\left\{\hat{\mathbf{E}}_1^H \hat{\mathbf{E}}_2 - z\hat{\mathbf{E}}_1^H \hat{\mathbf{E}}_1\right\}. \tag{28}$$

In this equation, the L roots of the polynomial $p(z)$ correspond to the generalized eigenvalues of the matrix,

$$\left\{\hat{\mathbf{E}}_1^H \hat{\mathbf{E}}_2,\ \hat{\mathbf{E}}_1^H \hat{\mathbf{E}}_1\right\}. \tag{29}$$

Algorithm 2 Search-Free (SF) DOA Estimation

1: **Input:** Snapshots $\{\mathbf{x}(t)\}$, linear array spacing d, wavelength λ, source number L
2: **Output:** Estimated DOAs $\{\hat{\theta}_\ell\}$
3: **Subspace Estimation:** Compute $\hat{\mathbf{R}}$, perform EVD, obtain signal subspace $\hat{\mathbf{E}}$
4: **Polynomial Formulation:** Using $z = e^{j\frac{2\pi d}{\lambda}\sin\theta}$, rewrite the SS residual determinant as a polynomial $F(z) = \sum_n c_n z^n$ with $\{c_n\}$ computed from $\hat{\mathbf{E}}_1, \hat{\mathbf{E}}_2$
5: **Root Processing:** Solve $F(z) = 0$ to obtain roots $\{z_k\}$, keep the L roots with $|z_k|$ closest to 1
6: **Angle Recovery:** For each selected root z_ℓ, compute $\hat{\theta}_\ell = \arcsin\left(\frac{\lambda}{2\pi d}\arg(z_\ell)\right)$

This reveals that, in the case of uniform array geometry, the proposed polynomial rooting method reduces to the standard DOA estimation algorithm. However, it is important to emphasize that the estimator presented in (26) is significantly more general than the classical DOA estimator. It supports non-uniform linear arrays, as long as the sensor displacement ratios x_m/x_1 can be related via a common rational basis. This broader applicability allows the proposed search-free generalized DOA estimation method to operate effectively in more diverse and flexible array configurations, thereby extending the practicality and utility of DOA estimation. The whole procedure of the proposed SF DOA estimation approach is summarized in Algorithm 2.

4.1. Computational Complexity Analysis

The computational complexity of the proposed spectral-search scheme can be analyzed as follows. First, it shares the same front-end cost as conventional subspace-based DOA estimators: forming the sample covariance matrix from K snapshots collected by a $2M$-element array requires on the order of $\mathcal{O}(KM^2)$ operations, and the subsequent eigenvalue decomposition (EVD) of a $2M \times 2M$ covariance matrix incurs a complexity of about $\mathcal{O}(M^3)$. After obtaining the signal subspace, it is partitioned into the submatrices $\hat{\mathbf{E}}_1$ and $\hat{\mathbf{E}}_2$, and for each candidate angle on a search grid of size G, the algorithm constructs the diagonal phase-rotation matrix $\mathbf{\Psi}(\theta)$, forms a residual matrix (e.g., $\mathbf{D}(\theta) = \hat{\mathbf{E}}_1^{\mathrm{H}}\hat{\mathbf{E}}_2 - \hat{\mathbf{E}}_1^{\mathrm{H}}\mathbf{\Psi}(\theta)\hat{\mathbf{E}}_1$), and evaluates a determinant-based spectral function. Since $\hat{\mathbf{E}}_1$ and $\hat{\mathbf{E}}_2$ are of size $M \times L$ with L typically small (number of sources), the per-angle cost is on the order of $\mathcal{O}(ML^2 + L^3)$, leading to a search-stage complexity of approximately $\mathcal{O}(GML^2)$. As a consequence, the overall complexity of the SS estimator grows linearly with the grid size G and thus with the desired angular resolution: very fine grids significantly increase the computational burden, even though the operations across different angles are relatively lightweight and can be parallelized.

In contrast, the search-free scheme retains the same front-end cost for covariance estimation and EVD, but it replaces the outer angular grid search with a single polynomial construction and root-finding procedure. Under the mild geometric assumptions on the linear array, the denominator of the SS spectral criterion is reformulated as a polynomial $p(z)$ in a complex exponential variable $z = e^{j\psi_1}$, whose coefficients are computed from $\hat{\mathbf{E}}_1$ and $\hat{\mathbf{E}}_2$ with a cost on the order of $\mathcal{O}(ML^2)$, which is comparable to evaluating the SS spectrum at a single grid point. The DOAs are then recovered from the L polynomial roots closest to the unit circle by applying a standard polynomial-rooting method, such as the eigen-decomposition of a companion matrix, which incurs roughly $\mathcal{O}(D^3)$ operations, where D denotes the polynomial degree, typically proportional to the effective aperture rather than any grid density. Importantly, the SF scheme's complexity does not depend on the angular grid size or resolution, and therefore, in scenarios where a high-resolution spectrum with a large G is required for the SS estimator, the SF scheme can achieve a substantially lower overall complexity while maintaining the same subspace accuracy and avoiding the computational overhead of exhaustive grid search.

5. Simulations Results and Discussions

In this part, we will present some simulation results to validate the effectiveness of the proposed two DOA estimation schemes. Specifically, a dual-subarray linear array structure is considered, where the number of sensors M varies from 3 to 15. The array is assumed to receive L uncorrelated narrowband signals from far-field sources, and the additive noise is modeled as spatially and temporally white Gaussian noise with unity variance at all sensors. The transmit signal-to-noise ratio (SNR) is varied from 0 dB to 25 dB to observe performance trends under different noise levels. Each simulation trial computes the root-mean-square error (RMSE) between the estimated and true DOAs over multiple Monte Carlo runs to ensure statistical reliability. For fair comparison, the same dataset and noise realizations are used for all schemes, including the two proposed SS and SF based DOA estimation schemes and the conventional MUSIC scheme which serves as a baseline.

Fig. 1 shows the RMSE performance of several direction-of-arrival estimation schemes versus the transmit SNR, where the number of sensors M is 5 and the conventional MUSIC scheme is used as a baseline. As shown in this figure, we can find that all three schemes exhibit an improved RMSE as

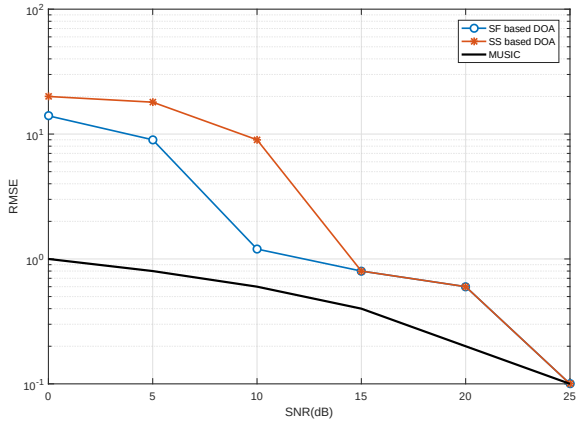

Figure 1. RMSE performance of several DOA estimation approaches versus SNR.

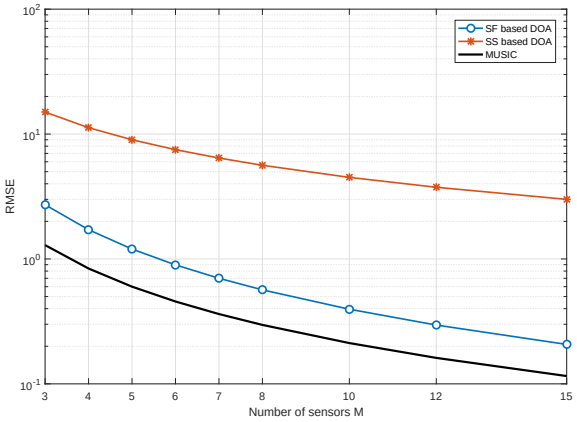

Figure 2. Effect of number of sensors M on the RSME of DOA estimation approaches.

the SNR increases from 0 dB to 25 dB, reflecting improved estimation accuracy at higher SNR levels. However, the proposed SF-based and SS-based DOA schemes consistently outperform MUSIC across the entire SNR range. When SNR is below 10 dB, both proposed schemes maintain significantly smaller RMSE than MUSIC, showing stronger robustness under noisy conditions. Around 10-15 dB, the RMSE of the SF-based DOA scheme is already below 1, whereas MUSIC remains around 10, indicating roughly an order-of-magnitude improvement. As SNR increases further beyond 20 dB, all schemes converge to low error levels, but the SF-based scheme achieves the lowest RMSE, slightly better than the SS-based one. These results demonstrate that the search-free polynomial-rooting approach not only reduces computational complexity but also achieves the highest estimation accuracy, while the spectral-search scheme still considerably outperforms the traditional MUSIC algorithm in terms of precision and stability across different SNR conditions.

Fig. 2 illustrates the RMSE performance of the several DOA estimation schemes versus the number of sensors M, where the transmit SNR is set to 10dB. We can find from Fig. 2 that all three schemes benefit from increasing the number of sensors, as the RMSE decreases monotonically with larger M, indicating an improved estimation accuracy due to enhanced array aperture and spatial resolution. However, the SF-based and SS-based DOA schemes consistently outperform the MUSIC algorithm across the entire range of M. For small-scale arrays ($M = 3 - 5$), MUSIC suffers from relatively large errors, with RMSE values exceeding 10, whereas both proposed schemes achieve substantially lower errors, roughly around 1 or less. As the number of sensors increases beyond $M = 8$, the gap between the proposed approaches and MUSIC becomes even more evident¡ªthe RMSE of the SF-based DOA drops below 0.5, while MUSIC still exhibits an RMSE several times higher. When $M \geq 12$, the SF-based and SS-based DOA curves converge toward very low RMSE, approaching the ideal limit, and the SF-based scheme slightly outperforms the SS-based one throughout. Overall, the results indicate that the proposed schemes scale more efficiently with array size, providing higher accuracy and robustness than MUSIC, and the search-free estimator achieves the best overall performance while maintaining lower computational complexity.

6. Conclusions

This paper studied a generalized dual-subarray linear array model with arbitrarily configurable inter-subarray displacement vectors and introduced two tailored subspace-based DOA estimation schemes. The first scheme, a spectral-search estimator, exploited the structured coupling between the signal subspaces of the two subarrays through a parametrized phase-rotation matrix. In this scheme, the DOAs were inferred by scanning over candidate angles that enforced rank deficiency in a residual matrix constructed from the estimated signal subspace, yielding a high-resolution spectrum that extended conventional methods with enhanced flexibility. The second scheme, a search-free (SF) estimator, operated under mild geometric constraints on the array and reformulated the same optimality criterion as a polynomial in a complex exponential variable, from which the DOAs were efficiently recovered via the roots closest to the unit circle, thereby removing the need for grid search and significantly lowering computational complexity. Simulation results in deterministic-network scenarios indicated that, for a (2×5)-element dual-subarray at moderate SNRs, the proposed SF estimator attained

an RMSE below 1, whereas the conventional MUSIC algorithm exhibited an RMSE on the order of 10, confirming an order-of-magnitude improvement in accuracy and highlighting the superior performance and scalability of both the SS and SF schemes.

References

[1] J. Steinwandt, F. Roemer, M. Haardt, and G. D. Galdo, "R-dimensional esprit-type algorithms for strictly second-order non-circular sources and their performance analysis," *IEEE Trans. Signal Process.*, vol. 62, no. 18, pp. 4824–4838, 2014.

[2] D. Oh, S. Kim, S. Yoon, and J. Chong, "Two-dimensional esprit-like shift-invariant TOA estimation algorithm using multi-band chirp signals robust to carrier frequency offset," *IEEE Trans. Wirel. Commun.*, vol. 12, no. 7, pp. 3130–3139, 2013.

[3] Q. Gu, H. Wang, W. Sun, T. Wu, and Y. Xu, "A sequential ESPRIT algorithm based on a novel UCSA configuration for parametric estimation of two-dimensional incoherently distributed source," *IEEE Trans. Veh. Technol.*, vol. 70, no. 1, pp. 356–370, 2021.

[4] S. Dai, "A generalization of rotational invariance for complex fuzzy operations," *IEEE Trans. Fuzzy Syst.*, vol. 29, no. 5, pp. 1152–1159, 2021.

[5] A. Bera, P. Klesk, and D. Sychel, "Constant-time calculation of zernike moments for detection with rotational invariance," *IEEE Trans. Pattern Anal. Mach. Intell.*, vol. 41, no. 3, pp. 537–551, 2019.

[6] H. Yu, R. Saleeb, P. A. Dalgarno, and D. D. Li, "Estimation of fluorescence lifetimes via rotational invariance techniques," *IEEE Trans. Biomed. Eng.*, vol. 63, no. 6, pp. 1292–1300, 2016.

[7] S. Tong, X. Yu, R. Li, K. Lu, Z. Zhao, and H. Zhang, "Alternate learning-based snr-adaptive sparse semantic visual transmission," *IEEE Trans. Wirel. Commun.*, vol. 24, no. 2, pp. 1737–1752, 2025.

[8] W. Niu, Y. Guo, X. Han, R. Ma, W. Zheng, X. Peng, and Z. Yang, "A high-frame-rate-imaging-based framework for moving point target detection in very low SNR," *IEEE Trans. Aerosp. Electron. Syst.*, vol. 61, no. 1, pp. 943–958, 2025.

[9] C. Yin, R. Zhang, Y. Li, Y. Ruan, T. Li, and J. Lu, "A recursion-based SNR determination method for short packet transmission: Analysis and applications," *IEEE Trans. Veh. Technol.*, vol. 74, no. 3, pp. 5205–5210, 2025.

[10] S. Deng and J. Han, "Signal periodic decomposition with conjugate subspaces," *IEEE Trans. Signal Process.*, vol. 64, no. 22, pp. 5981–5992, 2016.

[11] X. Xu, G. Li, and Y. Gu, "Unraveling the veil of subspace RIP through near-isometry on subspaces," *IEEE Trans. Signal Process.*, vol. 68, pp. 3117–3131, 2020.

[12] T. Blumensath, "Sampling and reconstructing signals from a union of linear subspaces," *IEEE Trans. Inf. Theory*, vol. 57, no. 7, pp. 4660–4671, 2011.

[13] C. Cao, H. Xiang, W. Song, H. Yi, F. Xiao, and X. Gao, "Lightweight multiscale neural architecture search with spectral-spatial attention for hyperspectral image classification," *IEEE Trans. Geosci. Remote. Sens.*, vol. 61, pp. 1–15, 2023.

[14] E. F. Collins, D. A. Roberts, and C. C. Borel, "Spectral mixture analysis of simulated thermal infrared spectrometry data: An initial temperature estimate bounded TESSMA search approach," *IEEE Trans. Geosci. Remote. Sens.*, vol. 39, no. 7, pp. 1435–1446, 2001.

[15] Q. Zhang, Y. Peng, Z. Zhang, and T. Li, "Semantic segmentation of spectral lidar point clouds based on neural architecture search," *IEEE Trans. Geosci. Remote. Sens.*, vol. 61, pp. 1–11, 2023.

[16] Y. He and G. Joseph, "Bayesian algorithms for kronecker-structured sparse vector recovery with application to IRS-MIMO channel estimation," *IEEE Trans. Signal Process.*, vol. 73, pp. 142–157, 2025.

[17] J. Wang, Q. Zhu, Z. Lin, Q. Wu, Y. Huang, X. Cai, W. Zhong, and Y. Zhao, "Sparse bayesian learning-based 3-d radio environment map construction - sampling optimization, scenario-dependent dictionary construction, and sparse recovery," *IEEE Trans. Cogn. Commun. Netw.*, vol. 10, no. 1, pp. 80–93, 2024.

[18] Z. Ren, L. Qiu, J. Xu, and D. W. K. Ng, "Sensing-assisted sparse channel recovery for massive antenna systems," *IEEE Trans. Veh. Technol.*, vol. 73, no. 11, pp. 17 824–17 829, 2024.

[19] J. Choi, "Performance limitation of closed-loop transmit antenna diversity over fast rayleigh fading channels," *IEEE Trans. Veh. Technol.*, vol. 51, no. 4, pp. 771–775, 2002.

[20] Y. Hu, A. Schmeink, and J. Gross, "Blocklength-limited performance of relaying under quasi-static rayleigh channels," *IEEE Trans. Wirel. Commun.*, vol. 15, no. 7, pp. 4548–4558, 2016.

[21] P. Cheng, M. Tao, Y. Xiao, and W. Zhang, "V-OFDM: on performance limits over multi-path rayleigh fading channels," *IEEE Trans. Commun.*, vol. 59, no. 7, pp. 1878–1892, 2011.

[22] Y. Cheng, T. Liu, J. Shi, D. Guan, Z. Liu, Y. Liu, and X. Li, "Generalized gridless formulation of reweighted $\ell _{2,1}$ minimization for doa estimation," *IEEE Trans. Aerosp. Electron. Syst.*, vol. 61, no. 2, pp. 2295–2308, 2025.

[23] X. Zhang, D. Feng, and W. Zheng, "Fast subspace and DOA estimation method for the case of high-dimensional and small samples," *IEEE Trans. Veh. Technol.*, vol. 74, no. 3, pp. 3958–3975, 2025.

[24] C. Yu, Y. Li, L. Li, Z. Huang, Q. Wu, and R. C. de Lamare, "Dual lawson norm-based robust DOA estimation for ris-aided wireless communication systems," *IEEE Trans. Aerosp. Electron. Syst.*, vol. 61, no. 1, pp. 582–592, 2025.

[25] X. Zhang, M. Hou, and Z. Hou, "Data-driven high-order point-to-point ILC with higher computational efficiency," *IEEE Trans Autom. Sci. Eng.*, vol. 21, no. 4, pp. 6011–6026, 2024.

[26] S. Lyu, X. Zhou, X. Wu, Q. Chen, and H. Chen, "Self-attention over tree for relation extraction with data-efficiency and computational efficiency," *IEEE Trans. Emerg. Top. Comput. Intell.*, vol. 8, no. 2, pp. 1253–1263, 2024.